NASA Contractor Report 190790
AIAA–92–3463

Anode Power Deposition in Applied-Field MPD Thrusters

Roger M. Myers
Sverdrup Technology, Inc.
NASA Lewis Research Center Group
Brook Park, Ohio

and

George C. Soulas
Ohio State University
Columbus, Ohio

Prepared for the
28th Joint Propulsion Conference and Exhibit
cosponsored by the AIAA, SAE, ASME, and ASEE
Nashville, Tennessee, July 6–8, 1992

Anode Power Deposition in Applied-Field MPD Thrusters

Roger M. Myers[1]
Sverdrup Technology, Inc.
NASA Lewis Research Center Group
Brook Park, OH 44142

George C. Soulas[2]
Ohio State University
Columbus, OH 43210

Abstract

Anode power deposition is the principal performance limiter of magnetoplasmadynamic (MPD) thrusters. Current thrusters loose between 50 and 70 percent of the input power to the anode. In this work, anode power deposition was studied for three cylindrical applied magnetic field thrusters for a range of argon propellant flow rates, discharge currents, and applied-field strengths. Between 60 and 95 percent of the anode power deposition resulted from electron current conduction into the anode, with cathode radiation depositing between 5 and 35 percent of the anode power, and convective heat transfer from the hot plasma accounting for less than 5 percent. While the fractional anode power loss decreased with increasing applied-field strength and anode size, the magnitude of the anode power increased. The rise in anode power resulted from a linear rise in the anode fall voltage with applied-field strength and anode radius. The anode fall voltage also rose with decreasing propellant flow rate. The trends indicate that the anode fall region is magnetized, and suggest techniques for reducing the anode power loss in MPD thrusters.

Nomenclature

A_{an}	anode surface area, m^2
A_c	cathode surface area, m^2
B_z	applied magnetic field strength, T
c	random thermal particle speed, m/s
D	length scale for convective heat transfer, m
E_{KE}	heavy particle kinetic energy, J
e	electron charge, C
F_{c-a}	cathode to anode view factor

---

[1]Propulsion Engineer, member AIAA

[2]graduate student, currently at
Sverdrup Technology, Inc.
NASA LeRC Group.

h_p	convective heat transfer coefficient for plasma, W/m^2K
J_d	discharge current, A
j_e	electron current density at anode, A/m^2
k	Boltzmann's constant, $1.38x10^{-23}$ J/K
k_p	plasma thermal conductivity, W/cm K
m_e	electron mass, kg
m_i	ion mass, kg
n_e	electron number density, m^{-3}
n_H	heavy particle number density, m^{-3}
P_a	anode power, W
P_{conv}	convective power density to anode, W/m^2
P_r^c	cathode radiation power density to anode, W/m^2
P_r^{pl}	plasma radiation power density to anode, W/m^2
Pr	Prandl number
R_a	anode radius, cm
Re	Reynolds' number
T_c	cathode surface temperature, K
T_e	electron temperature, K
u	flow velocity, m/s
V_{an}	anode fall voltage, V
ε	cathode emissivity
σ	Stefan-Boltzmann constant, 5.67×10^{-8} $W/m^2 K^4$
Φ	anode work function, eV
Λ	plasma parameter
Ω_e	electron Hall parameter

Introduction

The efficiency of magnetoplasmadynamic (MPD) thrusters must be increased by a factor of two if they are to successfully compete for application to spacecraft propulsion.[1,2] While MPD thrusters have demonstrated specific impulses over 5000 seconds and the ability to process several hundred kilowatts of power for periods of up to several hours, the currently attainable 25 percent thruster efficiency will likely preclude their use for spacecraft primary propulsion.

The low thruster efficiency results primarily from the large fraction of the input power deposited into the anode, which can range from 50 to 90 percent for thruster powers below one megawatt.[2-5] Reduction of this power loss will result in both performance improvements and system simplifications due to the decreased heat rejection requirements. Considerable effort has been expended to evaluate and reduce anode power deposition in MPD thrusters.[3-9] The studies include steady-state thrusters operated with and without applied magnetic fields on a variety of propellants at power levels from 5 to 50 kW, and quasi-steady tests[6,7] wherein the thruster is pulsed for 1 to 2 milliseconds, at power levels up to 20 MW. However, many of the steady-state

results were obtained at high facility pressures, which have been shown to strongly affect anode power deposition.[4] In addition, previous work failed to identify scaling parameters governing anode power deposition valid for a broad range of thruster geometries and operating conditions. At present the relationship between quasi-steady and steady-state test results is uncertain, and the lack of adequate scaling relationships precludes use of results obtained at thruster powers over one MW for improving thrusters operating at sub-megawatt power levels. The situation, however, is improving. Recent results with applied-field thrusters have shown that the anode power fraction decreased with increasing axial field strength and anode radius.[3,4] The anode power fraction also decreased with decreasing anode length and cathode radius. That work, however, did not address the impact of propellant flow rate or discharge current.

This paper presents the results of an effort to empirically establish the impact of thruster operating condition and geometry on the magnitude and mechanism of anode power loss. Measurements of anode power deposition were obtained across a broad range of propellant flow rates, discharge currents, and applied field strengths, for three applied-field MPD thruster geometries in an attempt to identify fundamental scaling relationships. Following a description of the experimental apparatus, anode power deposition measurements for the three thruster geometries are presented. The thruster operating conditions included argon flow rates from 0.025 to 0.14 g/s, discharge currents between 500 and 2000 amps, and applied field strengths from 0 to 0.2 T. The results were used to calculate the anode fall voltage, and scaling relationships for the anode fall were identified. Finally, a summary of results and potential approaches to reducing the anode power loss in MPD thrusters are presented.

Experimental Apparatus and Data Reduction

Thrusters and Applied-Field Magnets

A simplified thruster schematic is shown in Fig. 1. All three geometries tested consisted of a 0.64 cm radius, 2% thoriated tungsten cathode surrounded by a cylindrical water cooled copper anode. Anode radii of 2.54, 3.81, and 5.1 cm were tested. All electrodes were 7.6 cm long. Propellant was injected through a boron nitride plate at the back of the chamber via a 0.16 cm wide annulus at the cathode base and via twenty-four 0.16 cm diameter holes at the mid-radius between anode and cathode. All data presented here were obtained with an even split in propellant flow between the cathode annulus and the holes at the backplate mid-radius.

The need for plasma property measurements near the anode led to the design of a thruster permitting placement of electrostatic and pressure probes at the anode surface. This was accomplished by drilling 0.16 cm diameter holes through the walls of the water cooling channels as shown in Fig. 2. These diagnostics were only performed with the 3.81 cm radius anode thruster. Five of these diagnostic ports were drilled along the length of the anode at each of three azimuthal locations. The diagnostics used in this thruster are discussed below.

The MPD thrusters were mounted inside solenoidal coils (not shown in Fig. 1) used to generate a strong axial magnetic field in the thruster chamber and plume region. Two coil sizes were required to accommodate the different anode radii. The 2.54 and 3.81 cm radius anodes were tested using a magnet with a 15.3 cm diameter bore, the 5.1 cm radius anode required a magnet with a 20.3 cm bore diameter. Both coils were 15.3 cm wide (axially). The coils were made using

multiple turns of insulated copper tubing which carried both current and magnet cooling water.[4] Magnetic field calibrations showed that the coils produced fields which were azimuthally uniform to within 1%, with axial field strengths at the centerline of the coil exit plane of 1.66×10^{-4} T/A and 8.48×10^{-5} T/A for the 15.3 and 20.3 cm magnets, respectively. For all tests discussed in this report the thruster exit plane was flush with the downstream end of the coil, and quoted field strengths refer to values at the centerline of the coil exit plane (also the cathode tip). Field strengths at the coil center were twice the exit plane values.

Vacuum Facility and Test Stand

The MPD thrusters were tested in a 3 m diameter, 3 m long test port connected to a 7.6 m diameter, 21 m long vacuum facility via a 3 m diameter gate valve. A schematic of the test stand in the 3 m test port is shown in Fig. 3. The vacuum facility maintained a pressure below 0.07 Pa (5×10^{-4} torr) for all flow rates tested. Testing at varying pressures has shown that this pressure is low enough to ensure that the facility pressure did not impact the anode power deposition or thruster performance.[4] Additional details of this facility are available in Refs. 3, 4, and 10.

The thrusters were mounted on an inverted pendulum thrust stand capable of resolving thrust levels of 0.01 N.[10] Power and cooling water for the thruster and applied-field magnet passed through the thrust stand flexures. Calibrations over a broad range of operating conditions showed no thrust stand tares resulting from the water cooling, discharge current, or applied magnetic field.

Propellant was fed into the thrust chamber via two independent propellant feed lines. The propellant flow rates were measured using thermal conductivity flow type flow controllers with 2% precision. Periodic in situ calibrations were performed to ensure 2% accuracy.

Thruster and magnet cooling water was provided by two closed loop heat exchangers, each providing up to 0.5 kg/s of distilled water at a pressure of 0.83 MPa (120 psi). The water flow rate was measured using turbine flow meters which were calibrated periodically. The calibrations showed the flow rate measurements to be accurate to within 2 %. Type K thermocouples were imbedded a minimum of 7 cm into the water flow lines to measure the temperature rise across both the anode and cathode electrodes. The thermocouples were only accurate to +/- 0.5°K, which forced periodic adjustment of the water flow rate to ensure a minimum of 10°K temperature rise across the anode for all power levels tested. These steps ensured that the calorimetric measurements were accurate to within 5 %.

Anode Plasma Diagnostics

Both planar electrostatic probe and static pressure measurements were used to establish the plasma properties the surface of the 3.81 cm radius anode. The electrostatic probes consisted of 0.076 cm diameter tungsten wire inserted into a 0.15 cm diameter alumina tube. The tungsten wire tip was flush with the end of the alumina tube. The probe assembly was inserted through the steel tubes mounted on the 3.81 cm diameter anode (Fig. 2) and positioned such that the exposed tungsten surface was even with the anode surface. Note that at this position, the probes measure electron properties after the electrons have been accelerated through the fall region, and not the properties of the bulk plasma near the anode. The alumina tube-steel tube and alumina tube-

tungsten wire interfaces (outside anode) were covered with epoxy to provide a gas tight seal. Five electrostatic probes were used to obtain axial plasma property profiles. The probe circuit and data reduction techniques were identical to those used in Ref. 11, except that for these measurements the ion saturation current was subtracted from the probe current before the electron temperature and density were calculated. This improved the accuracy of the electron temperature measurements. Four capacitance manometers were used to measure the axial static pressure distribution along the anode. The manometers used had a pressure range of 0 to 1300 Pa with 0.1% precision. Teflon tubing 0.32 cm in diameter and 30 cm long was used to connect the steel tubes at the anode with the manometers.

Anode Fall Voltage Estimation

The equation used to calculate the anode fall voltage from the anode power measurements was derived by estimating the magnitudes of all the anode power deposition terms and eliminating those that are negligible. In general, the magnitude of the anode power can be written as:

$$P_a = \int_{A_{an}} (j_e(V_{an} + \frac{5kT_e}{2e} + \Phi) + P_r^c + P_{conv} + P_r^{pl})dA \qquad (1)$$

where the first term in the integral results from electron current conduction into the anode, the second represents the contribution from cathode radiation, the third term represents convective heat transfer from the hot plasma to the anode, and the fourth term represents plasma radiation reaching the anode surface. While the integral over the anode surface is required to allow for axial property gradients in the thruster chamber, no data currently exist which permit axial resolution of the bulk plasma properties near the anode. For this reason only average properties are discussed in this report.

Previous MPD thruster studies have indicated that the dominant heat transfer mechanism is the electron current conduction, which includes the anode fall voltage, the electron thermal energy in the bulk plasma at the edge of the fall region, and the anode work function. The plasma radiation consists of free-free, free-bound, and line radiation, which were shown to be negligible using relationships from Ref. 12 with the assumption of a fully ionized argon plasma at a temperature of 2 eV in the chamber. These assumptions are consistent with measurements obtained in the exit plane of steady-state[11] and quasi-steady[6,7,13] self- and applied-field MPD thrusters operated with argon propellant at power levels between 50 kW and 5 MW. Plasma convective heat transfer will be dominated by the neutral particle flux to the surface as the ions will be repelled by the anode fall voltage. Two approaches were used to estimate the magnitude of the convective power. The first, a simple kinetics calculation, yields a convective power of:

$$P_{conv} = \frac{n_H \bar{c}}{4} E_{KE} A_{an} \qquad (2)$$

where the heavy particle number density, n_H, was calculated using the one-dimensional continuity equation, the average neutral thermal speed was calculated assuming equal electron and neutral temperatures, and the kinetic energy per particle was calculated using the measured mass average plasma exhaust velocity. The results ranged from 1 - 3 kW for the conditions reported in this paper, values which are over an order-of-magnitude below the reported anode powers. The

assumed parameter values should yield a substantial overestimate of the convective power because the neutral density is thought to be less than 10% of the total density, and ions should be repelled from the anode by the positive anode fall voltage. In addition, the use of the exhaust velocity to estimate kinetic energies along the entire length of the anode is likely to overestimate the heavy particle kinetic energy because the average velocity in the chamber is lower than the exhaust velocity. Both of these issues are readdressed below using the anode plasma property measurements. The second method for convective power estimation used the formulation proposed by Saber[6] which assumes the heat transfer behaves as that of a flowing neutral gas. In this case the convective heat transfer coefficient is given by:

$$h_p = 0.026\frac{k_p}{D}\mathrm{Re}^{0.8}\mathrm{Pr}^{0.4} \tag{3}$$

where the Reynolds number, Prandl number, and plasma heat transfer coefficient were evaluated using transport coefficients from Ref. 11, the electron temperature was taken as 2.3×10^4 K, the plasma velocity was taken as 2×10^4 m/s, and the length scale D was taken to be the electrode length. The electron temperature and plasma velocity values are consistent with measurements reported previously.[4,11] These assumptions should yield an overestimate of the convective anode heat transfer. The convective heat flux was then estimated as:

$$P_{conv} = h_p T_e A_{an} \approx 200 \text{ W} \tag{4}$$

which is two to three orders of magnitude less than the anode powers reported in this paper. The above analyses clearly include many simplifying assumptions which require verification. In particular, use of the exhaust velocity in the first method above may actually underestimate the energy per particle in an applied-field thruster due to the presence of high azimuthal velocities. Observation of the anode surface for the larger thrusters indicates that the copper anode is being sputtered by propellant atoms moving in helical trajectories along the anode. Because the sputtering threshold of argon on a copper target is over 35 eV[14] (corresponding to a velocity of 1.3×10^4 m/s), this observation clearly indicates that high energy atoms or ions are striking the surface. Plasma velocity measurements near the anode surface are required to resolve this issue. For both methods of estimating convective power the resulting magnitudes are much smaller than the measured anode power losses.

Cathode radiation, on the other hand, clearly cannot be neglected. Measurements of cathode surface properties in steady-state thrusters[15] showed that the cathode temperature matched that required for thermionic emission of the discharge current, which for conditions reported in this paper corresponds to surface temperatures between 2900 and 3100 K. Cathode radiation deposited on the anode was estimated from:

$$P_r^c = F_{c-a}\varepsilon\sigma A_c T_c^4 \tag{5}$$

where the cathode to anode view factors, F_{c-a}, were calculated using the equations in Ref. 16. For a surface temperature of 3000 K, cathode radiation deposited between 4 and 7 kW into the anode for the electrode geometries tested. The anode surface temperature was neglected in the radiation exchange equation because the anode surface temperature was less than 1000 K for all operating conditions.

This analysis showed that the plasma convection and radiation terms in Eq. (1) can be neglected, but that the cathode radiation term must be included in the study of anode power deposition. Using these results, Eq. (1) was solved for the anode fall voltage in terms of the cathode radiation, electron temperature, and anode work function:

$$V_{an} = \frac{P_{an} - P_r^c}{J_d} - \left(\frac{5kT_e}{2e} + \Phi\right) \tag{6}$$

where the electron temperature of the bulk plasma near the anode was taken as 2.3×10^4 K and the work function of copper is 4.6 eV.

Results

The thruster operating envelopes were limited by both facility and thruster life considerations. Facility pumping speed limitations precluded testing at argon flow rates greater than 0.14 g/s, and the electrode heat exchangers could not absorb more than 80 kW. In addition, the thrusters would not operate stably with no applied magnetic field. Attempts to operate in a self-field mode always resulted in severe cathode and anode erosion characterized by particulate emission. The stable operating envelope also changed with thruster geometry. For example, while the 2.54 cm radius anode thruster operated very well with a propellant flow rate of 0.025 g/s, the 5.1 cm anode radius became unstable for flow rates below approximately 0.06 g/s. In general, increasing the thruster size shifted the stable operating envelope towards higher propellant flow rates and lower applied field strengths.

Data reported below include only conditions for which the thruster operated stably for several minutes. Measurements of cathode weight loss were taken for all tests, which showed that cathode mass loss rate was less than 0.5 % of the injected propellant flow rate in all cases. While some anode mass loss was evident in the thruster with the 5.1 cm radius anode, it was impossible to quantify due to the limited resolution of the mass balance.

Anode Power Measurements

Figures 4a - d show the anode power fractions as functions of applied magnetic field strengths for several discharge currents using the 2.54, 3.81, and 5.1 cm radius anodes. Figures 4c and 4d present results for argon flow rates of 0.10 and 0.14 g/s with the 5.1 cm radius anode, respectively. For all but one case the anode power fraction decreased with increasing applied field strength, though the values appear to approach an asymptote at the highest field strengths tested. The behavior of the one anomalous case, observed with the 5.1 cm radius anode at a discharge current of 750 A and an argon flow rate of 0.1 g/s (Fig. 4c), has not been explained, though thruster operation during that test was slightly erratic. In general, however, the anode power fraction decreased with increasing anode radius, with values ranging from a high of 0.75 with the 2.54 cm radius anode at low applied field strengths to a low of 0.50 with the 5.1 cm radius anode at the highest field strength that could be applied with that geometry. The anode power fraction decreased slightly with increasing discharge current. This result was confirmed by varying the discharge current at a constant field strength of 0.034 T for all three geometries (Fig. 5).

Following a relatively rapid decrease in anode power fraction (of between 12 and 18%) as the current was increased from 750 to 1250 A, the anode power fraction reached an asymptote, and even increased slightly for the three anode radii studied. The effect of propellant flow rate, on the other hand, was quite large (Figs. 6a - c). For all cases increasing flow rate decreased the anode power fraction, though the magnitude of the effect decreased as the anode radius increases. Most interesting is that the behavior of the anode power fraction as a function of applied-field strength changed completely with the 2.54 cm radius thruster when the flow rate was decreased from 0.050 to 0.025 g/s. At the lowest flow rate the anode power fraction increased, rather than decreased, with increasing field strength.

Anode Fall Voltage

Anode power deposition appears to be governed by the anode fall voltage. Using the techniques discussed above, the anode fall voltage was calculated from the calorimetric measurements of the anode power and estimates of the cathode radiation. Figures 7a - d show the variation in anode fall voltage with applied-field strength for several discharge currents for each of the three anode radii tested. Figures 7c and 7d present results for argon flow rates of 0.10 and 0.14 g/s, respectively, with the 5.1 cm radius anode. The anode fall voltages ranged from a low of -2 V for the 2.54 cm radius anode at a discharge current of 750 A and an applied field of 0.034 T, to a high of 42 V for the 5.1 cm anode with a discharge current of 1250 A and an applied field of 0.06 T. For all cases the anode fall voltage rose linearly with applied field strength. The slopes of the linear least-squares curve fits to the data are given in Table 1. There is only one case, the 5.1 cm radius anode with an argon flow of 0.10 g/s and a discharge current of 750 A, for which the discharge current had a major effect on the rate of anode fall voltage rise with applied field strength. This result indicates that the anomalous anode power fraction behavior observed in Figure 4c resulted from an increase in the anode fall voltage, not a change in bulk plasma characteristics. When the flow rate for the 5.1 cm radius anode was increased to 0.14 g/s (Fig. 7d, Table 1) the anomalous behavior at 750 A disappeared. While the discharge current did not appear to greatly affect the slopes of V_{an} vs. B_z, the minimum anode fall voltages, measured at the lowest applied field strengths for each geometry, clearly increased with increasing discharge current and anode radius. Values of the minimum anode falls are given in Table 2. The results for the 5.1 cm radius anode show that increasing the flow rate results in a large decrease in the minimum anode fall voltage.

The effect of discharge current at a constant applied-field strength is shown for the three anode radii in Fig. 8. The slopes of these curves can be viewed as the rate of increase in the minimum anode falls with discharge current in Fig. 7 and Table 2. Again it is apparent that the behavior of the largest anode at 750 A is anomalous, as for all other cases the anode fall rises linearly with discharge current. The slopes of the least-squares fits increase with increasing anode size. The effect of propellant flow rate on the slope of the V_{an} vs. J_d curve is shown for the 2.54 and the 5.1 cm radius anodes in Figs. 9a and b. The apparently anomalous data with the 5.1 cm radius thruster at 750 A and 0.10 g/s argon was not included in the least-squares curve fits. While the propellant flow rate affects both the slope and intercept with the smaller anode, it affects only the intercept with the larger one. The slope increase in Fig. 9a is in direct proportion to the change in flow rate.

The effect of propellant flow rate on the anode fall voltage was most dramatic when the magnetic field strength was varied. Figures 10a - c show plots of V_{an} vs. B_z for the three anode radii at several propellant flow rates. While the anode fall voltage increases linearly with applied-

field strength for all cases, the slope increases rapidly with decreasing flow rate for all but the large anode.

Anode Plasma Property Measurements

Electrostatic probes were used to obtain electron temperature and density measurements at five axial locations along the anode surface. A minimum of five complete probe current - voltage characteristics were obtained for each location and operating condition to verify reproducibility. If the probe signals were noisy the results were not included. Figures 11a and b show electron temperature and density measurements for three operating conditions as a function of axial distance from the chamber backplate. The electron temperature increased slightly toward the thruster exit plane, ranging from 3 to 4 eV near the backplate and from 4 to 5 eV near the exit plane. The electron density generally decreased toward the exit plane, though the one reliable data point obtained close to the backplate showed a sharp decrease in density at that location (Fig. 11b), possibly resulting from a low ionization fraction close to the propellant injection location. The electron temperature increased with applied-field strength, while the density decreased.

Pressure measurements obtained using capacitance manometers are plotted for the same operating conditions in Figure 12. Calculated values of the charged particle pressure, $2N_ekT_e$, obtained assuming equal electron and ion densities and temperatures, are also shown. The measured pressure drops rapidly toward the exit, decreasing from 65 Pa (0.5 torr) near the backplate to 5 Pa (0.03 torr) near the exit plane. The calculated charged particle pressure is relatively constant at about 5 Pa (0.03 torr) throughout the chamber. For the last two measured axial positions, at 5 and 6.2 cm from the backplate, the measured and calculated pressured are equal, indicating that the plasma was fully ionized at those locations. The measured pressure and calculated charged particle pressure indicate that the ionization fraction at the anode surface increases rapidly toward the exit plane. It was not possible to quantify the ionization fraction near the backplate due to the uncertainty in neutral particle temperature.

Discussion

The measured anode power levels and plasma properties substantiate the arguments used to eliminate the convective power term and show that cathode radiation is not a dominant source of anode power. First, given the uniform dependence of anode power on applied field strength it is likely that the same power deposition mechanisms control the anode power for all operating conditions. For Eq. (2) to predict the correct anode power magnitudes for all operating conditions, the flow velocity at the anode surface (either axial or azimuthal) would have to be up to 4 times the measured mass average exhaust speed obtained from thrust measurements.[3,4] This can be shown using Eq. (2) to calculate the ion speed required to deposit the highest measured anode power (60 kW). However, it appears from the pressure and density distributions at the anode surface that the plasma does not reach the exhaust velocity until near the exit plane. In addition, accelerating the propellant to speeds 4 times the exhaust speed would require more power than was actually put into the thruster. Similarly, for cathode radiation to dominate for all operating conditions the cathode temperature would have to be well over the melting point of tungsten at the higher power levels, whereas direct measurements indicate that the cathode surface temperature does not exceed 3200 K. These results reinforce the conclusion that electron current conduction into the anode is

the dominant source of anode power deposition. However, the relative magnitudes of the three terms governing this process, the anode fall voltage, electron thermal energy, and anode work function, change with the thruster operating condition. At low applied magnetic field strengths the electron thermal energy and anode work function are the dominant sources of anode power, with the anode fall voltage rising linearly with applied-field strength to dominate the anode power deposition at the higher field strengths. Note that the electron temperatures measured at the anode surface are not the same as that used in Eqs. (1) - (4) and (6). The values required for the equations are the electron temperature on the plasma side of the anode fall region, whereas the measurements were made at the anode surface, after the electrons had been accelerated across the fall region. The relatively high measured electron temperatures may indicate that some of the energy the electrons acquire across the fall is thermalized, though experimental error resulting from probe contamination could also result in high temperatures. The anode power fraction decrease with increased magnetic field shows that the voltage drop across the plasma increases more rapidly than the anode fall voltage.

The most prominent feature of the data presented above is the linear rise in anode fall voltage with applied magnetic field strength. For the flow rates studied, the rate of increase in anode fall voltage with applied field is insensitive to discharge current, appears to increase approximately linearly with anode radius, and is strongly dependent on propellant flow rate for the 2.54 and 3.81 cm anodes, but not for the 5.1 cm anode. The dependence of the V_{an} vs. B_z slope on anode radius is shown in Figure 13. While it is difficult to establish definite trends with only three anode radii, it appears that a linear fit explains most of the observed dependence. Examination of the behavior of the slopes with propellant flow rate did not reveal a quantitative relationship, though it appears that for the 2.54 cm anode the slope decreases as $\dot{m}^{-3/2}$. The relationship did not hold for the other anodes.

The linear rise of anode fall voltage with applied field strength indicates that the plasma in the anode region is magnetized.[3] Estimates of the electron Hall parameter, given by:

$$\Omega_e = \frac{4 \times 10^5 e B_z T_e^{1.5}}{m_e n_e \ln(\Lambda)} \qquad (7)$$

range from over 1 at the highest flow rate in the 2.54 cm radius thruster with the lowest applied-field strength to over 1000 with the lowest flow rate and the highest applied-field with the 5.1 cm radius anode. Thus, for almost all operating conditions the current carrying electrons will move along the magnetic field lines for many gyrations before undergoing a collision which allows them to move toward the anode. Recent studies on quasi-steady self-field thrusters have shown a correlation between the electron Hall parameter in the anode region and the anode fall voltage.[7] While this may explain the linear rise in fall voltage with applied field strength and with reducing propellant flow rate, the lack of a flow rate dependence with the large anodes is unexplained. The dominance of the applied-field over the self-induced magnetic fields for the thrusters studied in this work may explain the lack of a discharge current dependence, as the self-induced field has little effect on the Hall parameter.

The high electron Hall parameters lead to an increased anode fall voltage as a result of the higher electric field required to maintain a constant electron flux into the anode (discharge current). This effect could be mitigated by either reducing the Hall parameter near the anode surface or by changing the thruster geometry such that magnetic field lines cross the anode surface, thus

allowing electron motion along field lines to transport current into the anode. The first of these approaches could be accomplished by either tailoring the magnetic field shape or by judicious choice of propellant injection geometry. The former approach was recently attempted at Princeton University with mixed results,[17] though for some conditions there was a clear reduction in anode fall voltage. While anode propellant injection has been unsuccessfully attempted in the past,[18] the tests were performed at such high facility backpressures that the results are inconclusive. The effect of modifying the thruster and field geometries on anode power deposition has only received a cursory examination to date. Schall,[19] using a two-coil applied-field magnet, showed that modifying the field shape such that field lines crossed the anode surface reduced the anode fall voltage by as much as a factor of two. A similar reduction might be achieved by modifying the anode shape. For example, using an axially converging anode with an axial applied magnetic field would not only allow electron transport into the anode along magnetic field lines, but also may increase the plasma density near the anode surface, resulting in a decreased Hall parameter. The results presented in this report clearly show the importance of pursuing each of these approaches to reducing anode power deposition.

The negative anode fall voltages observed with the small anode for a propellant flow rate of 0.10 g/s and an applied field of 0.033 T indicate that for those conditions the random thermal electron current exceeds the discharge current.[20] Under those circumstances, the anode becomes negative with respect to the plasma so as to repel the excess electrons impinging on it. The minimum anode fall values in Table 2 show that these values increase monotonically with discharge current and anode radius. Figures 10a - c show that the minimum anode fall is inversely proportional to propellant flow rate for a given anode radius, a correlation which agrees with the dependence on anode radius at a constant propellant flow rate. This discussion leads to the following scaling relation for the minimum anode fall voltage:

$$V_{an,min} \propto \frac{J_d}{n\bar{c}} = \frac{J_d m_i R_a^2 u}{\dot{m}} \tag{8}$$

which appears to fit the available data. Note however, that the dependence on flow velocity, u, has not been directly observed experimentally.

Conclusions

Anode power and plasma characteristics measurements were made using three applied-field MPD thruster geometries over a wide range of operating conditions, including argon propellant flow rates between 0.025 and 0.14 g/s, discharge currents between 750 and 2000 A, and applied-field strengths between 0.033 and 0.2 T. Electron current conduction into the anode was shown to be the dominant source of anode power, with the electron thermal energy and anode work function contributions dominating at the low applied field strengths with the small anodes, and the anode fall voltage contribution dominating with the large anodes and higher applied-field strengths. The anode fall voltage was found to rise linearly with applied-field strength. Changes in discharge current did not have a significant effect on the rate of anode fall voltage rise with applied field strength , though the minimum anode fall voltage rose linearly with discharge current. Decreasing the propellant flow rate sharply increased the anode fall voltage, increasing both its magnitude and rate of increase with applied-field strength with the 2.54 and 3.81 cm radius anodes, while only increasing its magnitude for the 5.1 cm radius thruster. The anode fall behavior is consistent with

that expected for a magnetized fall region, and follows the behavior observed in quasi-steady, MW power level, self-field MPD thrusters. These conclusions show that the anode power deposition may be reduced by changing the anode and applied-field shape to allow for parallel current conduction into the anode, or adding propellant at the anode surface to decrease the electron Hall parameter in the anode region.

Acknowledgements

The authors would like to thank John Naglowsky, Larry Schultz, Jerry LaPlant, David Wolford, Peggy Yancer, John McAlea, Rob Butler, John Miller, Gerry Schneider, Bernard Loyer, Cliff Schroeder, David Wehrle, and Shawn Reese for their invaluable assistance during this project.

References

1. Sovey, J.S., and Mantenieks, M.A., "Performance and Lifetime Assessment of MPD Arc Thruster Technology," *Journal of Propulsion and Power*, Vol. 7, No. 1, Jan. - Feb. 1991, pp. 71-83.

2. Myers, R.M., Mantenieks, M.A., and LaPointe, M.R., "MPD Thruster Technology," AIAA Paper 91-3568, Sept. 1991; see also NASA TM 105242.

3. Myers, R.M., Mantenieks, M.A., and Sovey, J.S., "Geometric Effects in Applied-Field MPD Thrusters," AIAA Paper 90-2669, July 1990; see also NASA TM 103259.

4. Myers, R.M., "Applied-Field MPD Thruster Geometry Effects," AIAA Paper 91-2342, July 1991; see also NASA CR 187163.

5. Gallimore, A.D., Myers, R. M., Kelly, A.J., and Jahn, R.G., "Anode Power Deposition in an Applied-Field Segmented Anode MPD Thruster," AIAA Paper 91-2343, June 1991.

6. Saber, A. J., "Anode Power In a Quasi-Steady MPD Thruster," Ph.D. Dissertation, Princeton University, May 1974.

7. Gallimore, A.D., Kelly, A.J., and Jahn, R.G., "Anode Power Deposition in MPD Thrusters," IEPC Paper 91-125, 22nd International Electric Propulsion Conference, Viareggio, Italy, October 1991.

8. Shih, K. T., Pfender, E., Ibele, W.E., and Eckert, E.R.G., "Experimental Anode Heat Transfer Studies in a Coaxial Arc Configuration," *AIAA Journal*, Vol. 6, No. 8, August 1968, pp. 1482 - 1487.

9. Scheiderman, A., and Patrick, R. M., "Optimization of the Thermal Efficiency of the Magnetic Annular Arc," AIAA Paper 66-115, January 1966.

10. Haag, T.M., "Thrust Stand for High-Power Electric Propulsion Devices," *Rev. Sci. Instrum.*, Vol. 62, No. 5, May 1991, pp.1186-1191.

11. Myers, R.M., Wehrle, D., Vernyi, M., Biaglow, J., and Reese, S., "A Preliminary Characterization of Applied-Field MPD Thruster Plumes," AIAA Paper 91-2339, June 1991; see also NASA CR 187165.

12. Mitchner, M., and Kruger, C.H., Partially Ionized Gases, John Wiley &Sons, New York, N.Y., 1973, pp. 295 - 304.

13. Nakayama, T., Toki, K., and Kuriki, K., "Quantitative Imaging of MPD Flowfields," IEPC 88-088, 20th International Electric Propulsion Conference, Garmish-Partenkirchen, Germany, October 1988.

14. Henscheke, E.B., and Derby, S.E., "Full-Plane Threshold Energies for Cathode Sputtering of Metals with Ar+ Ions", *Journal of Applied Physics*, Vol. 34, No. 8., Aug. 1963, pp. 2458-2467.

15. Myers, R.M., Suzuki, N., Kelly, A.J., and Jahn, R.G., "Cathode Phenomena in a Low-Power Magnetoplasmadynamic Thruster," *Journal of Propulsion and Power*, Vol. 7, No. 5, Sept.-Oct. 1991, pp. 760-766.

16. Siegel, R., and Howell, J. R., Thermal Radiation Heat Transfer, 2nd edition, Hemisphere Publ. Corp., New York, New York, 1981.

17. Gallimore, A.D., Kelly, A.J., and Jahn, R.G., "Anode Power Deposition in an MPD Thruster with a Magnetically Annulled Hall Parameter Anode," AIAA Paper 92-3461, July 1992.

18. Merke, W.D., Auweter-Kurtz, M., Habiger, H., Kurtz, H., and Schrade, H.O., "Nozzle Type MPD Thruster Experimental Investigations," IEPC 88-028, 20th International Electric Propulsion Conference, Garmisch-Partenkirchen, Germany, Oct. 1988.

19. Schall, W., "Influence of Magnetic Fields on Anode Losses in MPD Arcs," AIAA Paper 72-502, April 1972.

20. Merinov, N., et al. , "Anode Processes with a Negative Potential Drop at the Anode," *Soviet Physics - Technical Physics*, Vol. 21, No. 4, April 1976, pp. 467 - 472.

Anode Radius cm	Argon Flow Rate g/s	Anode Fall Voltage vs. Applied Field Strength Slope V/T			
		750 A	1000 A	1250 A	1500 A
2.54	0.10	142	152	148	167
3.81	0.10	237	370	270	
5.1	0.10	1653	495	503	
5.1	0.14	490	503	470	

Table 1. Effect of anode radius and discharge current on V_{an} vs. B_z slope.

Anode Radius cm	Argon Flow Rate g/s	Minimum Anode Fall Voltage V			
		750 A	1000 A	1250 A	1500 A
2.54	0.10	- 2.0	- 1.0	2.0	4.0
3.81	0.10	6.0	8.0	12	
5.1	0.10	14	17	23	
5.1	0.14	6.0	8.0	15	

Table 2 - Effect of geometry and discharge current on the anode fall voltage at the minimum applied-field strength for each geometry.

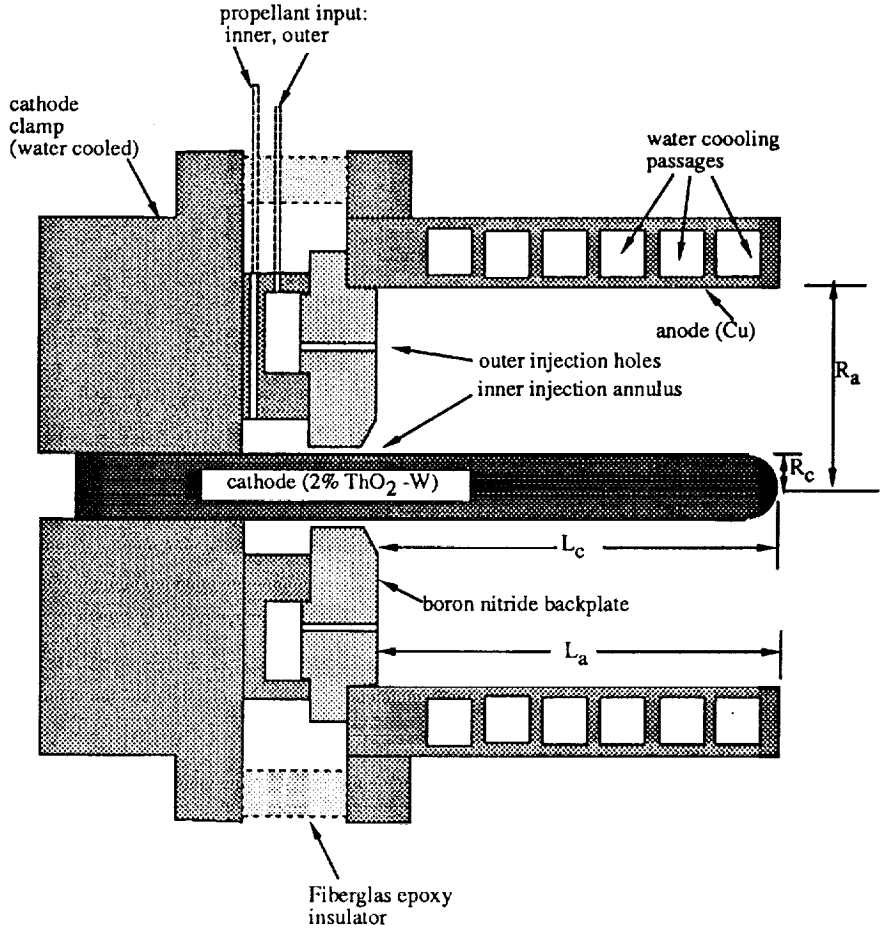

Fig. 1 MPD thruster schematic. Anode radii of 2.54, 3.81, and 5.10 cm were tested.

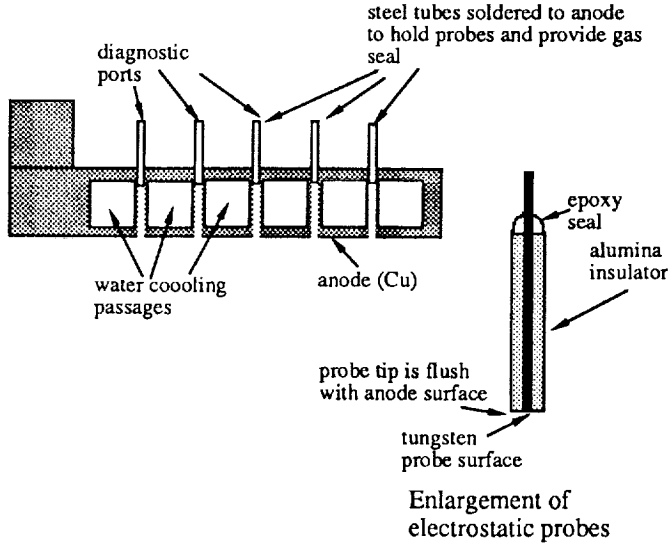

Fig. 2 MPD thruster anode plasma diagnostic port and probe details. R_a = 3.81 cm

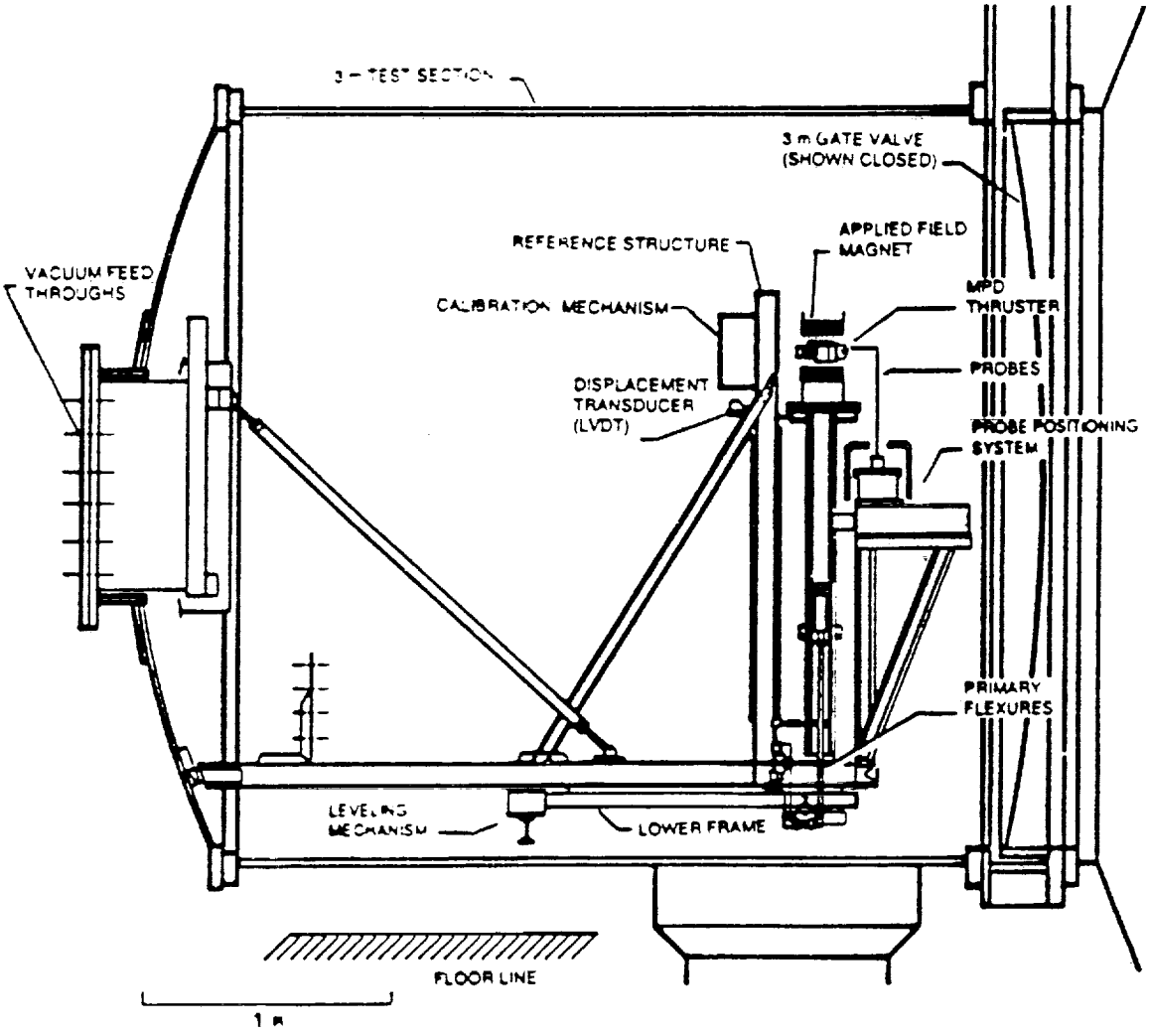

Fig. 3 MPD thruster test stand schematic.

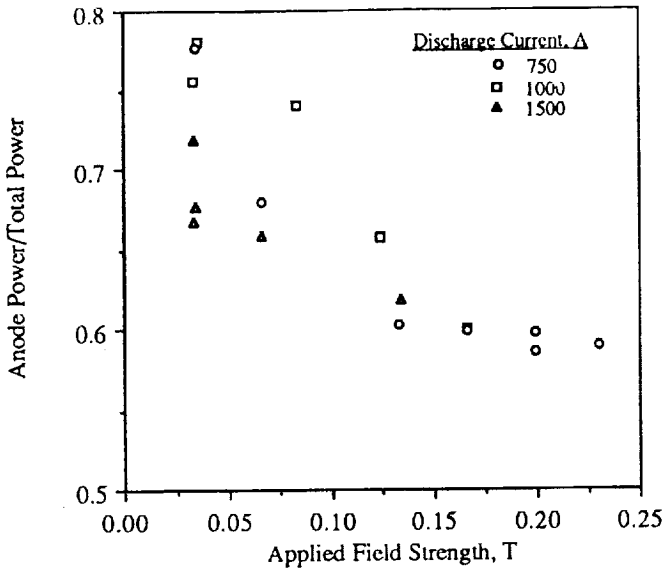

a. R_a = 2.54 cm, 0.10 g/s argon.

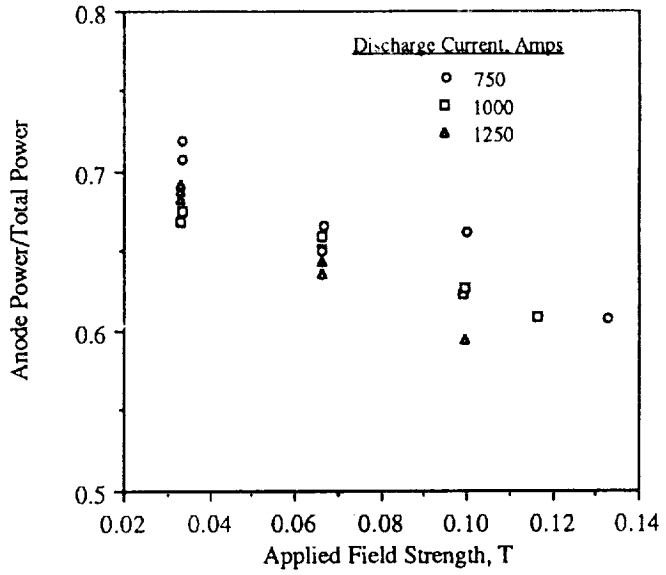

b. R_a = 3.81 cm, 0.10 g/s argon.

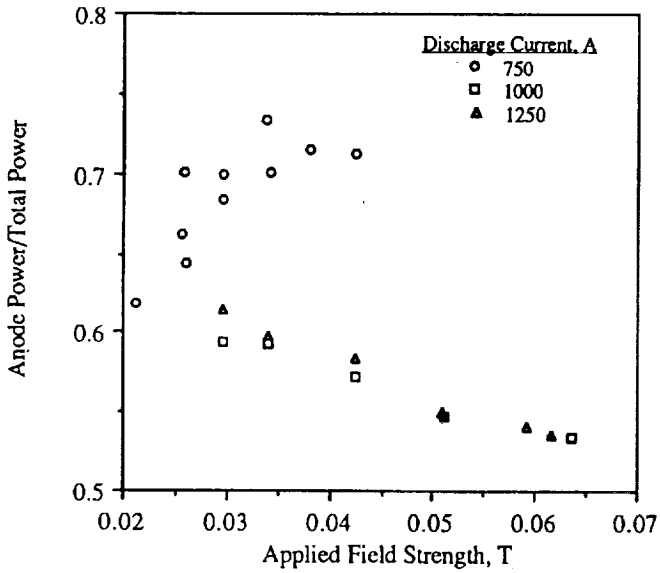

c. R_a = 5.1 cm, 0.10 g/s argon.

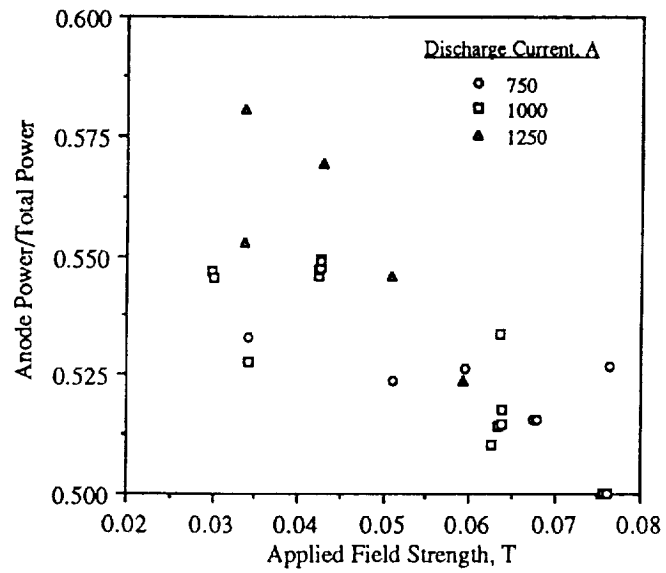

d. R_a = 5.1 cm, 0.14 g/s argon.

Fig. 4 Anode power fraction vs. applied magnetic field strength for 3 anode radii at several discharge currents each.

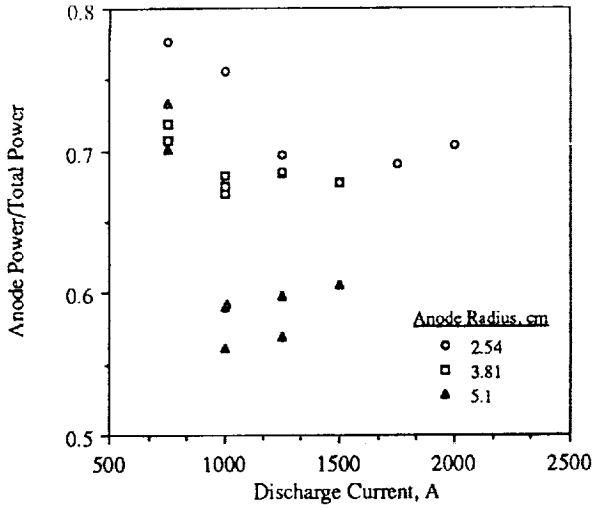

Fig. 5 Anode power fraction vs. discharge current for 3 anode radii at an applied field strength of 0.034 T. Argon flow rate of 0.10 g/s.

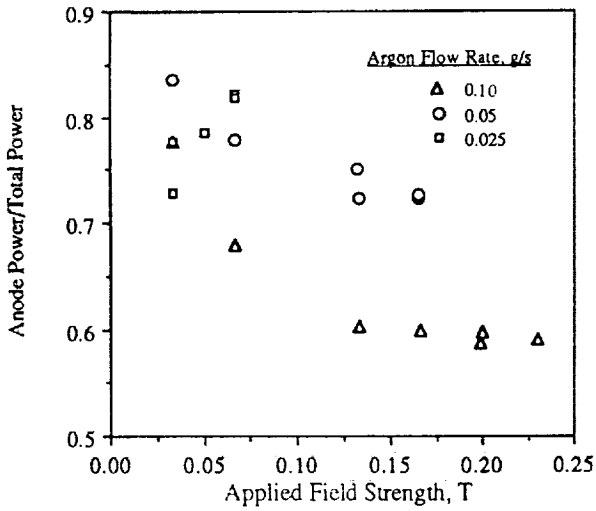

a. R_a = 2.54 cm, J_d = 750 A.

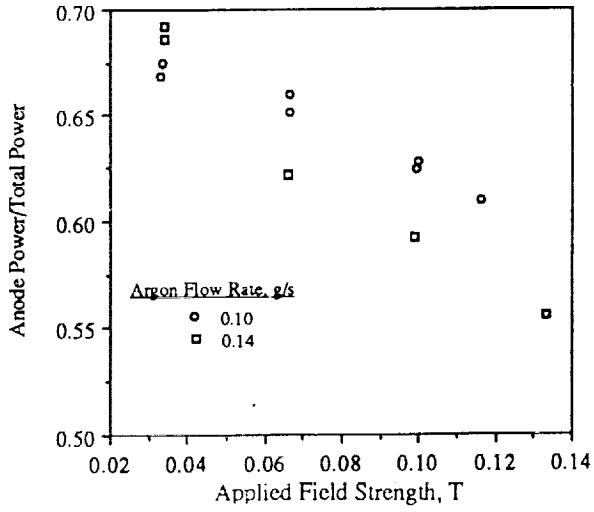

b. R_a = 3.81 cm, J_d = 1000 A.

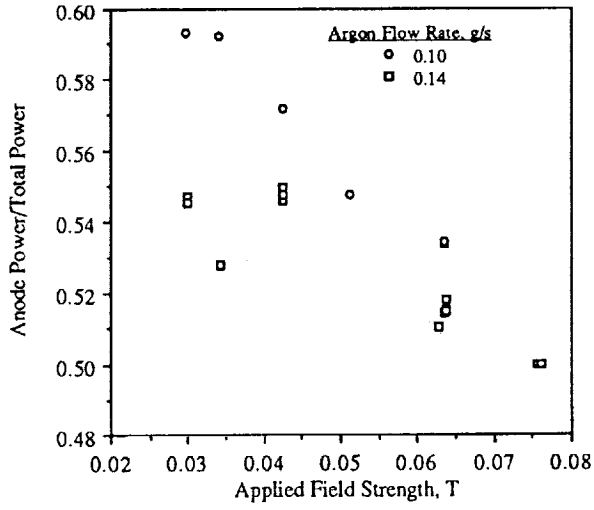

c. R_a = 5.1 cm, J_d = 1000 A.

Fig. 6 Anode power fraction vs. applied field strength for 3 anode radii with several argon flow rates.

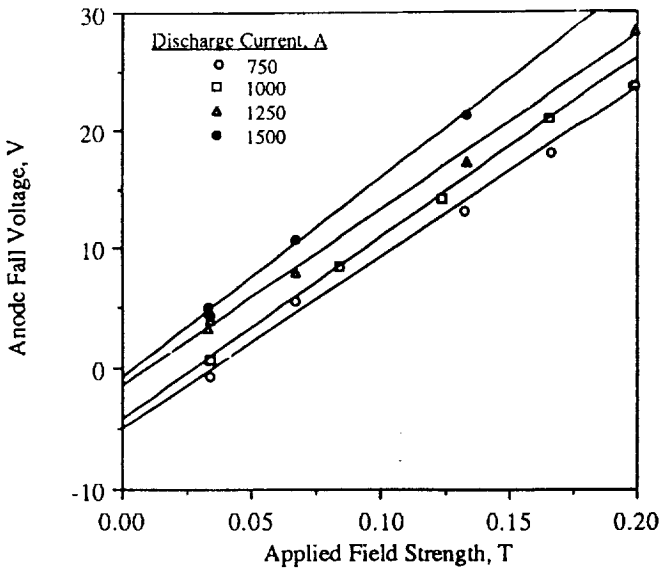

a. R_a = 2.54 cm, 0.10 g/s argon.

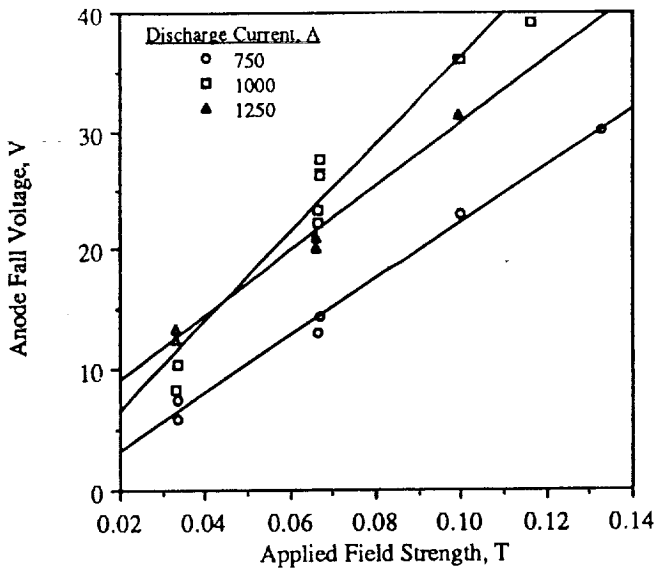

b. R_a = 3.81 cm, 0.10 g/s argon.

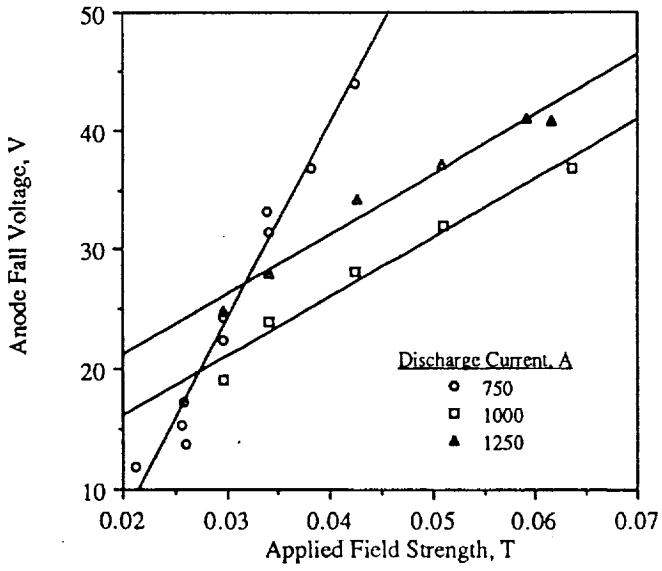

c. R_a = 5.1 cm, 0.10 g/s argon.

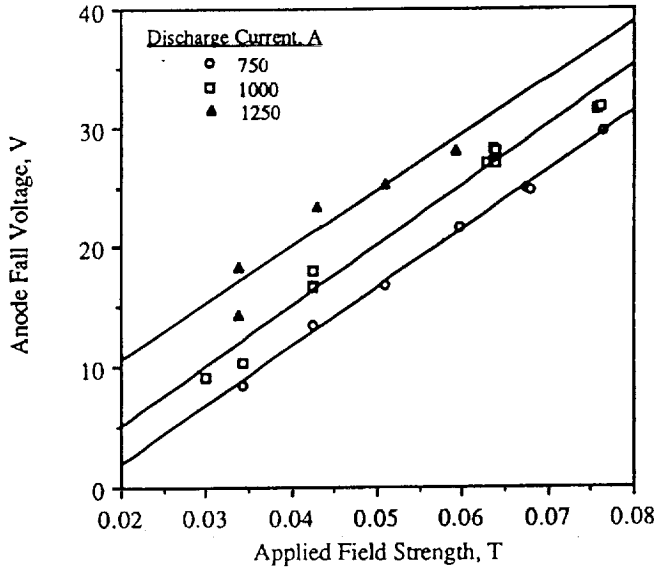

d. R_a = 5.1 cm, 0.14 g/s argon.

Fig. 7 - Anode fall voltage vs. applied field strength for the three anode radii at several discharge currents each.

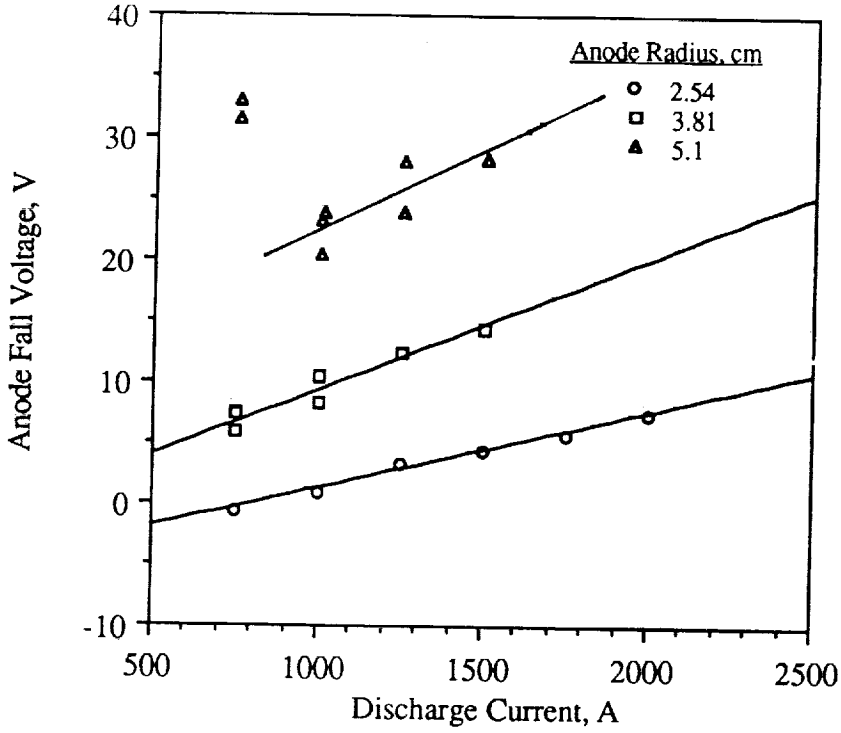

Fig. 8 - Anode fall voltage vs. discharge current for the three anode radii at a flow rate of 0.1 g/s and an applied field strength of 0.034 T.

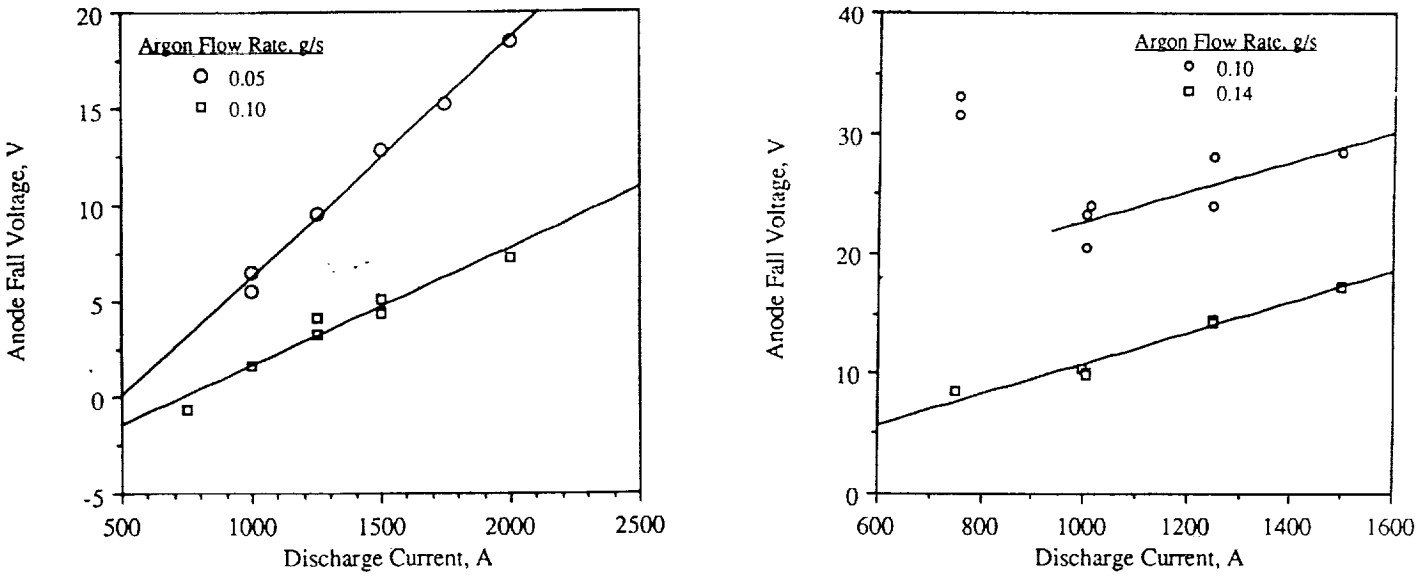

a. R_a = 2.54 cm

b. R_a = 5.1 cm

Fig. 9 - Anode fall voltage vs. discharge current for the three anode radii at several argon flow rates with an applied field strength of 0.034 T.

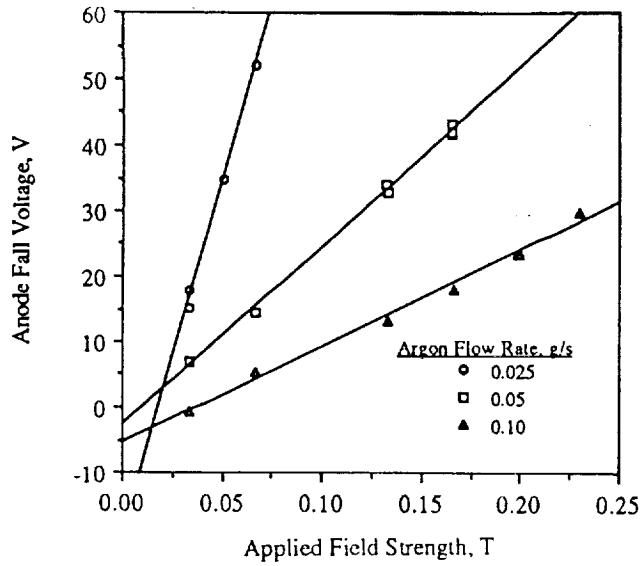

a. R_a = 2.54 cm, J_d = 750 A.

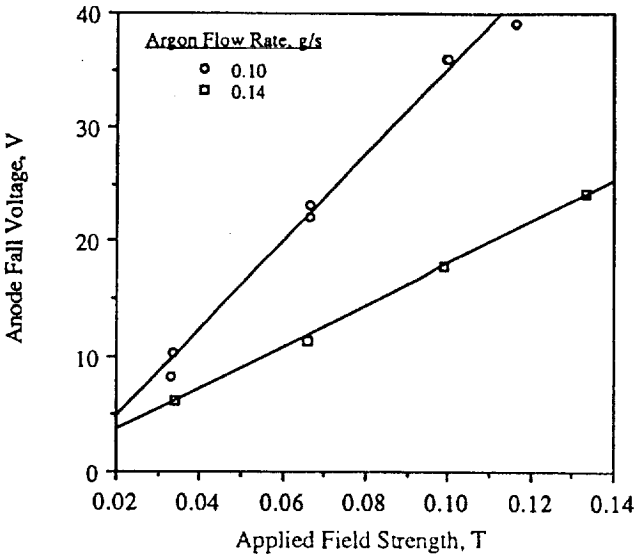

b. R_a = 3.81 cm, J_d = 1000 A.

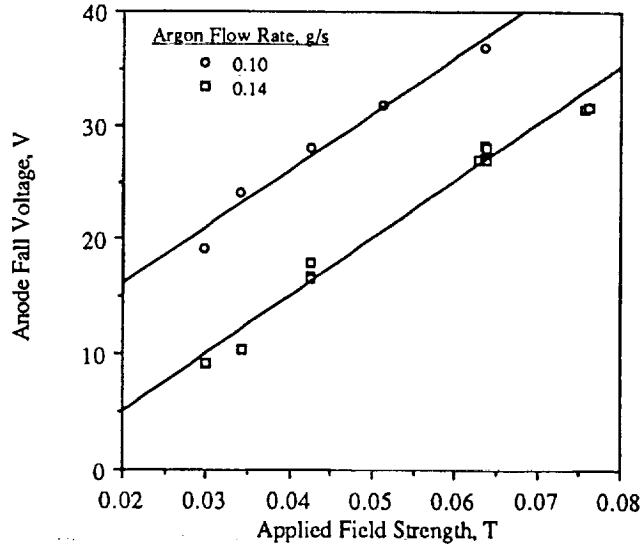

c. R_a = 5.1 cm, J_d = 1000 A.

Fig. 10 - Anode fall voltage vs. applied field strength for the three anode radii at several argon flow rates.

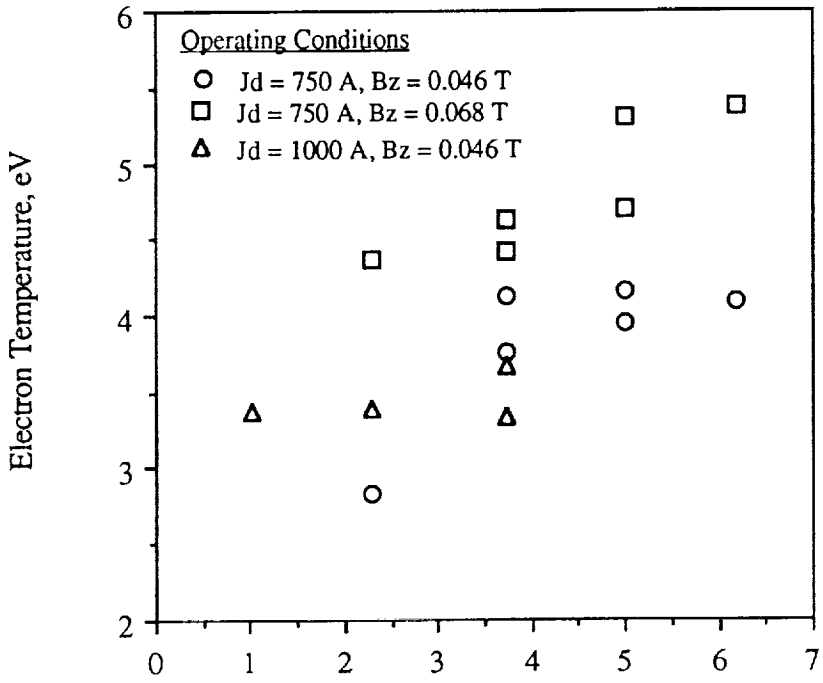

a. Electron Temperature

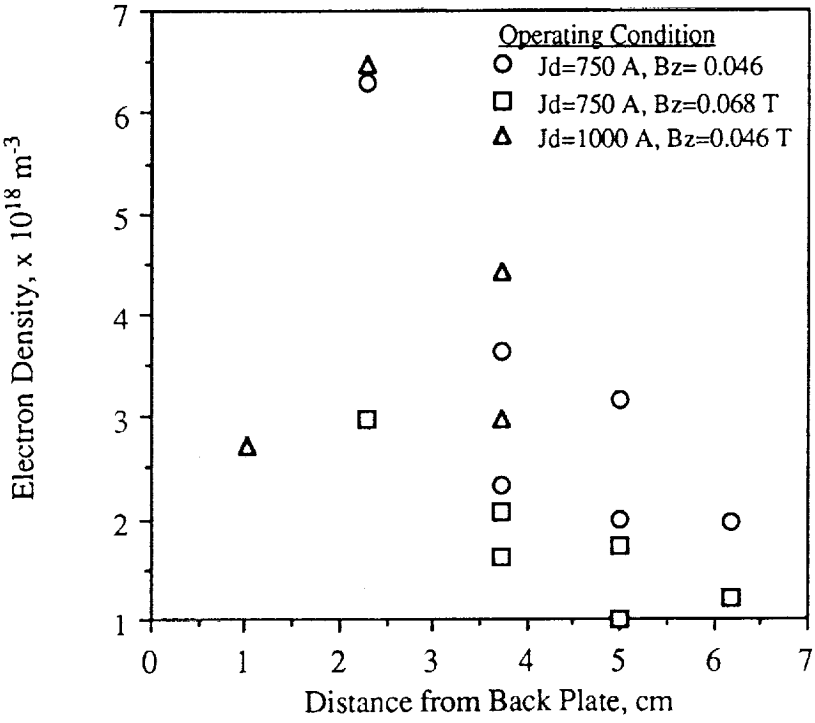

b. Electron Density

Figure 11 - Axial electron temperature and density distributions for 3.81 cm radius anode at an argon flow rate of 0.10 g/s.

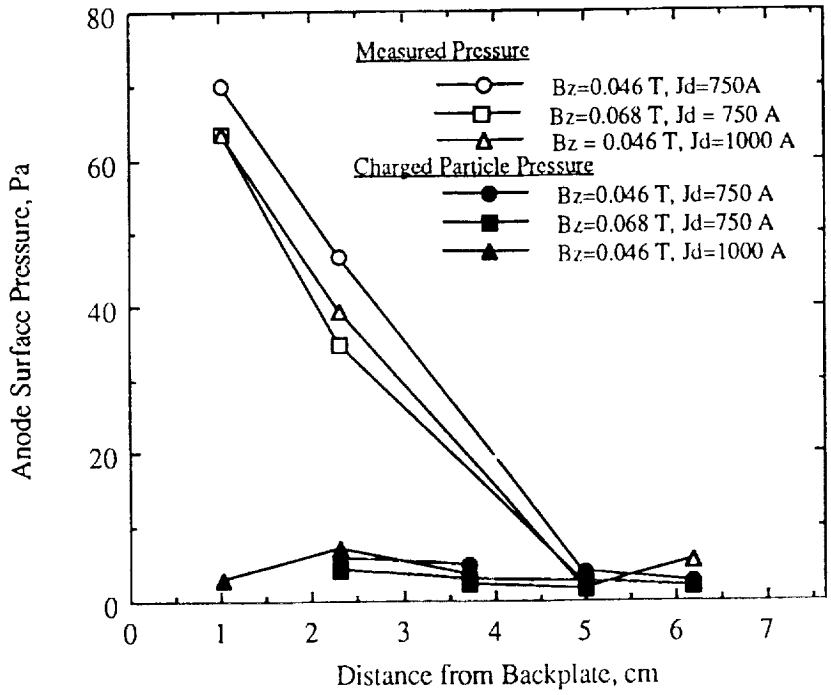

Figure 12 - Measured static pressure and calculated charged particle pressure distributions for 3.81 cm radius anode at an argon flow rate of 0.10 g/s.

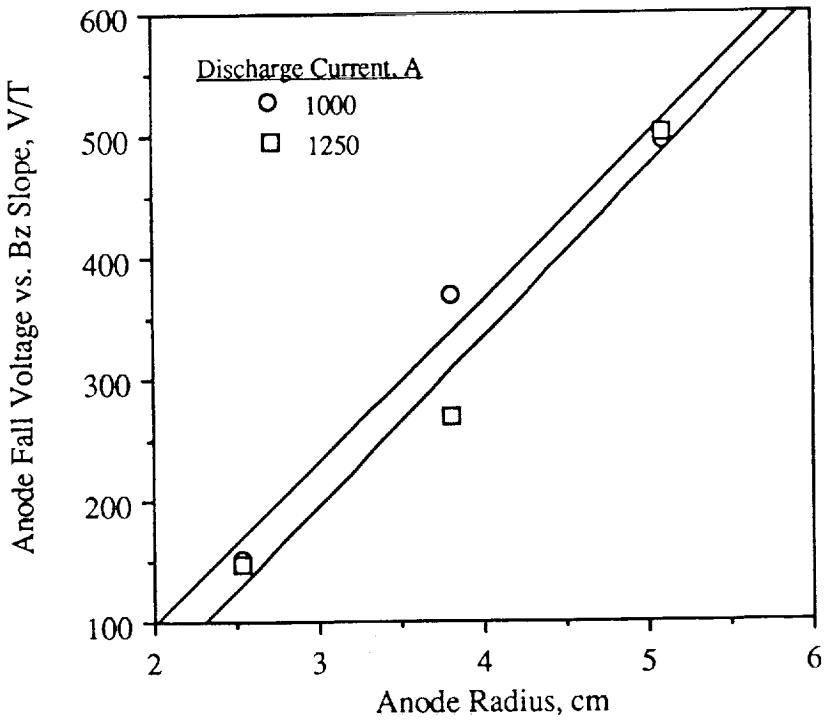

Figure 13 - Rate of increase of anode fall voltage with applied magnetic field strength as a function of anode radius. 0.10 g/s argon flow rate.

REPORT DOCUMENTATION PAGE

Form Approved
OMB No. 0704-0188

1. AGENCY USE ONLY (Leave blank)	2. REPORT DATE	3. REPORT TYPE AND DATES COVERED
	July 1992	Final Contractor Report

4. TITLE AND SUBTITLE

Anode Power Deposition in Applied-Field MPD Thrusters

5. FUNDING NUMBERS

WU-506-32-31

6. AUTHOR(S)

Roger M. Myers and George C. Soulas

7. PERFORMING ORGANIZATION NAME(S) AND ADDRESS(ES)

Sverdrup Technology, Inc.
Lewis Research Center Group
2001 Aerospace Parkway
Brook Park, Ohio 44142

8. PERFORMING ORGANIZATION REPORT NUMBER

E-7404

9. SPONSORING/MONITORING AGENCY NAMES(S) AND ADDRESS(ES)

National Aeronautics and Space Administration
Lewis Research Center
Cleveland, Ohio 44135-3191

10. SPONSORING/MONITORING AGENCY REPORT NUMBER

NASA CR-190790
AIAA-92-3463

11. SUPPLEMENTARY NOTES

Project Manager, James S. Sovey, (216) 433-7454.

12a. DISTRIBUTION/AVAILABILITY STATEMENT

Unclassified - Unlimited
Subject Category 20, 75

12b. DISTRIBUTION CODE

13. ABSTRACT *(Maximum 200 words)*

Anode power deposition is the principal performance limiter of magnetoplasmadynamic (MPD) thrusters. Current thrusters loose between 50 and 70 percent of the input power to the anode. In this work, anode power deposition was studied for three cylindrical applied magnetic field thrusters for a range of argon propellant flow rates, discharge currents, and applied-field strengths. Between 60 and 95 percent of the anode power depositions resulted from electron current conduction into the anode, with cathode radiation depositing between 5 and 35 percent of the anode power, and convective heat transfer from the hot plasma accounting for less than 5 percent. While the fractional anode power loss decreased with increasing applied-field strength and anode size, the magnitude of the anode power increased. The rise in anode power resulted from a linear rise in the anode fall voltage with applied-field strength and anode radius. The anode fall voltage also rose with decreasing propellant flow rate. The trends indicate that the anode fall region is magnetized, and suggest techniques for reducing the anode power loss in MPD thrusters.

14. SUBJECT TERMS

Electric propulsion; Plasma dynamics

15. NUMBER OF PAGES

24

16. PRICE CODE

A03

17. SECURITY CLASSIFICATION OF REPORT	18. SECURITY CLASSIFICATION OF THIS PAGE	19. SECURITY CLASSIFICATION OF ABSTRACT	20. LIMITATION OF ABSTRACT
Unclassified	Unclassified	Unclassified	